

Received April 2, 2019, accepted April 23, 2019, date of publication April 29, 2019, date of current version May 7, 2019.

Digital Object Identifier 10.1109/ACCESS.2019.2913747

Non-Iterative DOA Estimation Using Discrete Fourier Transform Interpolation

YUAN CHEN¹, ANNIE HIN CHEUNG KO², WING SHAN TAM³, (Senior Member, IEEE),
CHI WAH KOK³, (Senior Member, IEEE), AND HING CHEUNG SO⁴, (Fellow, IEEE)

¹School of Computer & Communication Engineering, University of Science and Technology Beijing, Beijing 100083, China

²School of Professional Education and Executive Development, The Hong Kong Polytechnic University, Hong Kong

³Canaan Semiconductor Ltd., Hong Kong

⁴Department of Electronic Engineering, City University of Hong Kong, Hong Kong

Corresponding authors: Chi Wah Kok (eekok@ieee.org) and Hing Cheung So (hcsso@ee.cityu.edu.hk)

This work was supported in part by the National Natural Science Foundation of China under Grant 61701021, and in part by the Fundamental Research Funds for the Central Universities under Grant FRF-TP-17-017A2.

ABSTRACT A fast and accurate non-iterative direction-of-arrival (DOA) estimation algorithm for multiple targets in additive white Gaussian noise is devised in this paper. The proposed estimator makes use of the two highest magnitudes discrete Fourier transform (DFT) coefficients of the input data and two of their associated neighboring bins, resulting in a deterministic complexity of $\mathcal{O}(N(1 + \log(N)))$ with N being the number of sensors. The bias and mean squares error of the DOA estimates are analyzed. The simulation results are presented to validate the correctness of theoretical derivation and demonstrate the superiority of the devised estimator over several conventional DOA estimators.

INDEX TERMS Direction-of-arrival, single snapshot, interpolation, discrete Fourier transform.

I. INTRODUCTION

Direction-of-arrival (DOA) estimation can be found in numerous areas such as single-input single-output [1], multiple-input single-output radar/sonar range-Doppler imaging [2] and array processing [3]–[8], which refers to accurately finding the locations of sources using a finite set of noisy observations in terms of either parametric or nonparametric methodologies [9], [10]. In the former one, the signal is assumed to be described as a known function, and no assumptions are made on the signal in the latter approach. The parametric algorithms usually allow the derivation of the optimal estimators, but the performance may deteriorate when the assumed signal model and actual one are mismatched. Although the nonparametric ones may not provide the optimum estimation performance, it can be utilized in more applications even when there is no prior knowledge of the signal.

Classical nonparametric methods such as Capon [11]–[13], multiple signal classification (MUSIC) [14], [15] and estimation of signal parameters via rotation invariance techniques (ESPRIT) [16] are popular solvers. However, they involve extensive computational cost because peak searching

is required. Amplitude and phase estimator (APES) is suggested in [17] and [18], which can accurately locate multiple sources using multiple snapshots. Although these methods can obtain accurate DOA estimation in the case of high signal-to-noise ratio (SNR) or numerous snapshots, their computational complexity is very high.

To alleviate the computational complexity problem, discrete Fourier transform (DFT) on noisy measurements can be applied. Several two-step algorithms have been suggested [19]–[21], where the coarse DOA estimates determined in the DFT step are refined in the second step by a spectral peak interpolation method in the spectral domain. Although the two-step approach can achieve high estimation accuracy with low computational complexity, it has not yet been applied to multiple-target DOA estimation. In [22], the observed time-domain sequence is first preprocessed by different windows, and the largest-magnitude and its neighbors of the DFT coefficients of windowed data are utilized to provide an unbiased estimation. Candan [23] proposes an unbiased DFT interpolation method, which employs the Taylor series expansion (TSE) on the largest-magnitude DFT coefficient and the neighbor bins. As the approximation of TSE is utilized, it cannot be extended to the multiple-target DOA estimation directly. Furthermore, [24] suggests an iterative interpolation method, which uses all DFT coefficients.

The associate editor coordinating the review of this manuscript and approving it for publication was Xianpeng Wang.

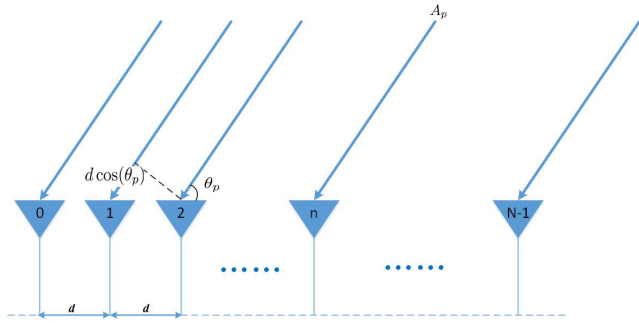


FIGURE 1. Illustration of uniform linear array.

For existing interpolation methods, they are devised according to the single-target model and thus cannot be applied directly to multiple-target scenario. A DOA estimator known as non-iterative fast method (NIFM) is devised in this paper, which can estimate the DOAs with low and deterministic complexity. A two-target scenario is taken as an illustration, which can be applied in the area of the long linear microphone array [25]. Our method is based on the two-step approach provided in [26], where the fine-tune procedure is realized by interpolation. A new DFT interpolation criterion is developed in Section II for multiple-target case, such that the proposed method only requires the two spectral peaks and two of their neighboring bins to provide accurate DOA estimates. The two-target scenario is taken as an example to illustrate the algorithm. The performance of the NIFM is analyzed in Section III by the application of TSE on the DFT spectral interpolation equations derived in Section II. Theoretical analysis of the estimation bias and mean squares error (MSE) is provided. The discussion of the algorithm computational complexity is also included. Computer simulation results are presented in Section IV, which demonstrate the accurate estimation performance and the very low computational complexity of the developed method when compared with the methods by Jacobsen and Candan, MUSIC and ESPRIT. Finally, conclusions are drawn in Section V.

II. PROPOSED METHOD

Without loss of generality, we consider a uniform linear array (ULA) [27] with N well-calibrated and identically-polarized sensors, where P uncorrelated narrow-band source targets impinge from far field. Then the p -th target, referred to as A_p , is taken as an illustration in Figure 1. The observed single-snapshot data of the n -th sensor, denoted by y_n , can be modeled as:

$$y_n = \sum_{p=1}^P A_p e^{-j2\pi nd \cos(\theta_p)/\lambda} + q_n, \quad n = 0, 1, \dots, N - 1, \quad (1)$$

where $\theta_p \in [0^\circ, 180^\circ)$ is the azimuth angle corresponding to the p -th target, λ denotes the wavelength, d is the distance between two adjacent sensors with the value of $\lambda/2$ [28] and

q_n is the independent identically distributed (IID) complex noise term following the zero-mean white Gaussian distribution with unknown variance σ^2 . Our task is estimating $\{\theta_p\}_{p=1}^P$ from observations $\{y_n\}_{n=0}^{N-1}$. Let $\varpi_p = -\pi \cos(\theta_p)$, the signal model in (1) can be rewritten as

$$y_n = \sum_{p=1}^P A_p \exp(j\varpi_p n) + q_n. \quad (2)$$

Since ϖ_p and θ_p are one-to-one mapping relationship, the DOA estimation task is converted to finding $\{\varpi_p\}_{p=1}^P$ from observations $\{y_n\}_{n=0}^{N-1}$.

Consider the N -DFT on $\{y_n\}_{n=0}^{N-1}$. The k -th DFT coefficient, referred to as Y_k , is expressed as

$$Y_k = \sum_{n=0}^{N-1} y_n \exp(-j\omega_k n), \quad = S_k + Q_k, \quad k = 0, 1, \dots, N - 1. \quad (3)$$

The signal component is given by

$$S_k = \sum_{p=1}^P A_p \exp\left(j\frac{\varpi_p - \omega_k}{2}(N - 1)\right) \frac{\sin\left(\frac{\varpi_p - \omega_k}{2}N\right)}{\sin\left(\frac{\varpi_p - \omega_k}{2}\right)}, \quad (4)$$

where $\omega_k = -\pi + \frac{2\pi k}{N}$ and Q_k denote the noise components associated with the DFT coefficients. Let L_p ($p = 1, 2, \dots, P$) be the P largest-magnitude peak indices among $\{Y_k\}_{k=0}^{N-1}$, so that the true values of ϖ_p are represented as

$$\varpi_p = -\pi + \frac{2\pi(L_p + \delta_p)}{N}, \quad p = 1, 2, \dots, P, \quad (5)$$

where $-0.5 \leq \delta_p \leq 0.5$ denote the offsets between the index of ϖ_p from the bins at L_p , respectively. Since $\{L_p\}_{p=1}^P$ are obtained according to DFT, the task is now converted to estimate $\{\delta_p\}_{p=1}^P$ from observations $\{y_n\}_{n=0}^{N-1}$. Employing (4)–(5), the DFT coefficient S_k corresponding to m -th ($m = 1, 2, \dots, P$) peak and its neighbors has the form of

$$S_{L_m} = \sum_{p=1}^P \left\{ A_p \exp\left(j\frac{\pi(N - 1)}{N}(L_{pm} + \delta_p)\right) \bullet \frac{\sin\left(\pi(L_{pm} + \delta_p)\right)}{\sin\left(\frac{\pi}{N}(L_{pm} + \delta_p)\right)} \right\}, \quad (6)$$

$$S_{L_{m-1}} = \sum_{p=1}^P \left\{ A_p \exp\left(j\frac{\pi(N - 1)}{N}(L_{pm} + \delta_p + 1)\right) \bullet \frac{\sin\left(\pi(L_{pm} + \delta_p + 1)\right)}{\sin\left(\frac{\pi}{N}(L_{pm} + \delta_p + 1)\right)} \right\}, \quad (7)$$

$$S_{L_{m+1}} = \sum_{p=1}^P \left\{ A_p \exp\left(j\frac{\pi(N - 1)}{N}(L_{pm} + \delta_p - 1)\right) \bullet \frac{\sin\left(\pi(L_{pm} + \delta_p - 1)\right)}{\sin\left(\frac{\pi}{N}(L_{pm} + \delta_p - 1)\right)} \right\}, \quad (8)$$

where $L_{pm} = L_p - L_m$ and \bullet denote the scalar product operator. In the scenario of large N , with the use of the fact that

$\exp(\pi(K+x)) \sin(\pi(K+x)) = \exp(\pi x) \sin(\pi x)$, (6)–(8) can be simplified as

$$S_{L_m} = \sum_{p=1}^P \frac{A_p \exp(j\pi \delta_p) \sin(\pi \delta_p)}{\sin\left(\frac{\pi}{N}(L_{pm} + \delta_p)\right)}, \quad (9)$$

$$S_{L_m-1} = \sum_{p=1}^P \frac{A_p \exp(j\pi \delta_p) \sin(\pi \delta_p)}{\sin\left(\frac{\pi}{N}(L_{pm} + \delta_p + 1)\right)}, \quad (10)$$

$$S_{L_m+1} = \sum_{p=1}^P \frac{A_p \exp(j\pi \delta_p) \sin(\pi \delta_p)}{\sin\left(\frac{\pi}{N}(L_{pm} + \delta_p - 1)\right)}. \quad (11)$$

Furthermore, (9)–(11) are

$$\begin{aligned} & \prod_{\ell=1}^P \sin\left(\frac{\pi}{N}(L_{\ell m} + \delta_{\ell})\right) S_{p_m} \\ &= \sum_{p=1}^P A_p \exp(j\pi \delta_p) \sin(\pi \delta_p) \prod_{\ell \neq p} \sin\left(\frac{\pi}{N}(L_{\ell m} + \delta_{\ell})\right), \end{aligned} \quad (12)$$

$$\begin{aligned} & \prod_{\ell=1}^P \sin\left(\frac{\pi}{N}(L_{\ell m} + \delta_{\ell} + 1)\right) S_{p_m-1} \\ &= \sum_{p=1}^P A_p \exp(j\pi \delta_p) \sin(\pi \delta_p) \prod_{\ell \neq p} \sin\left(\frac{\pi}{N}(L_{\ell m} + \delta_{\ell} + 1)\right), \end{aligned} \quad (13)$$

$$\begin{aligned} & \prod_{\ell=1}^P \sin\left(\frac{\pi}{N}(L_{\ell m} + \delta_{\ell} - 1)\right) S_{p_m+1} \\ &= \sum_{p=1}^P A_p \exp(j\pi \delta_p) \sin(\pi \delta_p) \prod_{\ell \neq p} \sin\left(\frac{\pi}{N}(L_{\ell m} + \delta_{\ell} - 1)\right). \end{aligned} \quad (14)$$

According to the product-to-sum property of trigonometric functions, there exists three coefficients a_0 , a_1 and a_2 such that

$$\begin{aligned} & a_1 \prod_{\ell=1}^P \sin\left(\frac{\pi}{N}(L_{\ell m} + \delta_{\ell})\right) S_{p_m} \\ &+ a_2 \prod_{\ell=1}^P \sin\left(\frac{\pi}{N}(L_{\ell m} + \delta_{\ell} + 1)\right) S_{p_m-1} \\ &= a_0 \prod_{\ell=1}^P \sin\left(\frac{\pi}{N}(L_{\ell m} + \delta_{\ell} - 1)\right) S_{p_m+1}. \end{aligned} \quad (15)$$

To illustrate the problem clearly, we take two targets as an illustration, where $P = 2$. Let L_1 and L_2 ($0 < L_1 < L_2 < N - 1$) be the two largest-magnitude peak indices among $\{Y_k\}_{k=0}^{N-1}$, such that the true values of ϖ_1 and ϖ_2 are represented as

$$\varpi_1 = -\pi + \frac{2\pi(L_1 + \delta_1)}{N}, \quad (16)$$

$$\varpi_2 = -\pi + \frac{2\pi(L_2 + \delta_2)}{N}, \quad (17)$$

where $-0.5 \leq \delta_1, \delta_2 \leq 0.5$ denote the offsets between the true values from the bin values at L_1 and L_2 , respectively. As L_1 and L_2 are straightforwardly obtained by DFT, the estimation task is converted to finding δ_1 and δ_2 . Let $\Delta\delta = \delta_2 - \delta_1$ and $L = L_2 - L_1$. Considering the first two terms in (3), the DFTs on $\{s_n\}_{n=0}^{N-1}$ with peaks at S_{ϖ_1} and S_{ϖ_2} are

$$S_{\varpi_1} = A_1 N + A_2 \frac{\exp\left(j\left(\frac{N-1}{2N}\pi\Delta\delta - \frac{\pi}{N}L\right)\right) \sin(\pi\Delta\delta)}{\sin\left(\frac{\pi}{N}(\Delta\delta + L)\right)}, \quad (18)$$

$$S_{\varpi_2} = A_2 N + A_1 \frac{\exp\left(-j\left(\frac{N-1}{2N}\pi\Delta\delta - \frac{\pi}{N}L\right)\right) \sin(\pi\Delta\delta)}{\sin\left(\frac{\pi}{N}(\Delta\delta + L)\right)}. \quad (19)$$

It can be seen from (18) and (19) that S_{ϖ_p} ($p = 1, 2$) are influenced by both ϖ_1 and ϖ_2 . Note that the existing interpolation schemes with assumption of single-target model cannot provide the satisfactory estimation performance since they ignore this information.

In the absence of noise term Q_k , the first peak and its neighboring bins, namely, L_1 -th, $(L_1 - 1)$ -th and $(L_1 + 1)$ -th DFT coefficients, are given by

$$Y_{L_1} = \frac{\gamma_1}{\sin\left(\frac{\pi\delta_1}{N}\right)} + \frac{\gamma_2}{\sin\left(\frac{\pi(L+\delta_2)}{N}\right)}, \quad (20)$$

$$Y_{L_1-1} = \exp\left(-\frac{j\pi}{N}\right) \left(\frac{\gamma_1}{\sin\left(\frac{\pi(\delta_1+1)}{N}\right)} + \frac{\gamma_2}{\sin\left(\frac{\pi(L+\delta_2+1)}{N}\right)} \right), \quad (21)$$

$$Y_{L_1+1} = \exp\left(\frac{j\pi}{N}\right) \left(\frac{\gamma_1}{\sin\left(\frac{\pi(\delta_1-1)}{N}\right)} + \frac{\gamma_2}{\sin\left(\frac{\pi(L+\delta_2-1)}{N}\right)} \right). \quad (22)$$

where

$$\gamma_1 = A_1 \exp\left(j\pi\delta_1 \frac{N-1}{N}\right) \sin(\pi\delta_1), \quad (23)$$

$$\gamma_2 = B_2 \exp\left(j\pi\delta_2 \frac{N-1}{N}\right) \sin(\pi\delta_2), \quad (24)$$

and $B_2 = A_2 \exp(-j\pi \frac{L}{N})$. Then (20)–(22) satisfy

$$\begin{aligned} & \sin\left(\frac{\pi(\delta_1+1)}{N}\right) \sin\left(\frac{\pi(L+\delta_2+1)}{N}\right) \exp\left(\frac{j\pi}{N}\right) Y_{L_1-1} \\ &+ \sin\left(\frac{\pi(\delta_1-1)}{N}\right) \sin\left(\frac{\pi(L+\delta_2-1)}{N}\right) \exp\left(-\frac{j\pi}{N}\right) Y_{L_1+1} \\ &= 2 \cos\left(\frac{\pi}{N}\right) \sin\left(\frac{\pi\delta_1}{N}\right) \sin\left(\frac{\pi(L+\delta_2)}{N}\right) Y_{L_1}. \end{aligned} \quad (25)$$

Similarly, the neighbors of the L_2 -th bin satisfy the following relationship:

$$\begin{aligned} & \sin\left(\frac{\pi(\delta_1 + 1 - L)}{N}\right) \sin\left(\frac{\pi(\delta_2 + 1)}{N}\right) \exp\left(\frac{j\pi}{N}\right) Y_{L_2-1} \\ & + \sin\left(\frac{\pi(\delta_1 - 1 - L)}{N}\right) \sin\left(\frac{\pi(\delta_2 - 1)}{N}\right) \exp\left(\frac{-j\pi}{N}\right) Y_{L_2+1} \\ & = 2 \cos\left(\frac{\pi}{N}\right) \sin\left(\frac{\pi(\delta_1 - L)}{N}\right) \sin\left(\frac{\pi\delta_2}{N}\right) Y_{L_2}. \end{aligned} \quad (26)$$

Let $\mu_1 = \tan\left(\frac{\pi\delta_1}{N}\right)$ and $\mu_2 = \tan\left(\frac{\pi\delta_2}{N}\right)$. Knowing that μ_1 and μ_2 are real numbers, therefore, we can consider the real part of the DFT coefficients alone as

Employing the product-to-sum formulas of trigonometric functions on (25)–(26), we have

$$\begin{aligned} r_0 &= \text{Re}\{Y_{L_1}\}, \quad \ell_0 = \text{Re}\{Y_{L_2}\}, \\ r_1 &= \text{Re}\left\{\exp\left(j\frac{\pi}{N}\right) Y_{L_1-1}\right\}, \\ r_2 &= \text{Re}\left\{\exp\left(-j\frac{\pi}{N}\right) Y_{L_1+1}\right\}, \\ \ell_1 &= \text{Re}\left\{\exp\left(j\frac{\pi}{N}\right) Y_{L_2-1}\right\}, \\ \ell_2 &= \text{Re}\left\{\exp\left(-j\frac{\pi}{N}\right) Y_{L_2+1}\right\}, \\ C_1 &= \tan\left(\frac{\pi}{N}\right), \quad C_2 = \tan\left(\frac{\pi(L+1)}{N}\right), \\ C_3 &= \tan\left(\frac{\pi(L-1)}{N}\right), \quad C_4 = \tan\left(\frac{\pi L}{N}\right), \\ D_1 &= \cos\left(\frac{\pi L}{N}\right), \quad D_2 = \cos\left(\frac{\pi(L+1)}{N}\right), \\ D_3 &= \cos\left(\frac{\pi(L-1)}{N}\right), \quad B = \frac{2D_1}{D_2 D_3}, \end{aligned} \quad (28)$$

where $\text{Re}\{x\}$ denotes the real part of x . To remove the term $\mu_1\mu_2$, (27), as shown at the bottom of this page can be simplified as two quadratic equations, which are

$$\mu_2^2 (\mathbf{x}^T \mathbf{A} \mathbf{z}) + \mu_2 (\mathbf{x}^T \mathbf{B} \mathbf{z}) + \mathbf{x}^T \mathbf{C} \mathbf{z} = 0, \quad (30)$$

$$\mu_1^2 (\mathbf{x}^T \mathbf{D} \mathbf{z}) + \mu_1 (\mathbf{x}^T \mathbf{W} \mathbf{z}) + \mathbf{x}^T \mathbf{Q} \mathbf{z} = 0, \quad (31)$$

where (32)–(38), shown at the top of the next page.

Solving (30) and (31) using the roots of quadratic equation allows us to estimate μ_1 and μ_2 , namely, $\hat{\mu}_1$ and $\hat{\mu}_2$ as

$$\hat{\mu}_2 = \frac{-\mathbf{x}^T \mathbf{B} \mathbf{z} + \sqrt{(\mathbf{x}^T \mathbf{B} \mathbf{z})^2 - 4(\mathbf{x}^T \mathbf{A} \mathbf{z})(\mathbf{x}^T \mathbf{C} \mathbf{z})}}{2(\mathbf{x}^T \mathbf{A} \mathbf{z})}, \quad (39)$$

$$\hat{\mu}_1 = \frac{-\mathbf{x}^T \mathbf{W} \mathbf{z} + \sqrt{(\mathbf{x}^T \mathbf{W} \mathbf{z})^2 - 4(\mathbf{x}^T \mathbf{D} \mathbf{z})(\mathbf{x}^T \mathbf{Q} \mathbf{z})}}{2(\mathbf{x}^T \mathbf{D} \mathbf{z})}. \quad (40)$$

Since $|\mu_1|$ and $|\mu_2|$ ($|\mu_1|, |\mu_2| < \tan\left(\frac{\pi}{2N}\right)$) are small, we select the smaller root as the estimates.

After $\hat{\mu}_1$ and $\hat{\mu}_2$ have been estimated, combining (27)–(40), as shown at the bottom of this page, the estimates of θ_1 and θ_2 , referred to as $\hat{\theta}_1$ and $\hat{\theta}_2$, are then:

$$\hat{\theta}_1 = \cos^{-1}\left(1 - \frac{2L_1}{N} - 2\frac{\tan^{-1}(\hat{\mu}_1)}{\pi}\right), \quad (41)$$

$$\hat{\theta}_2 = \cos^{-1}\left(1 - \frac{2L_2}{N} - 2\frac{\tan^{-1}(\hat{\mu}_2)}{\pi}\right). \quad (42)$$

To further improve the performance, we divide δ_1 or δ_2 into different subranges without additional computational complexity. Actually, we can divide the subrange into any ranges, however, increasing the number of subranges will also result in the higher computational complexity, which is not desirable. Taking nine subranges as an example, the accuracy and computational cost will be as high as performing the algorithm twice. Since the iterative application of the proposed algorithm is equivalent to using more subranges, we choose dividing the offset into three subranges.

To choose the subrange, it must satisfy three conditions: first, the union of all subranges should cover the whole ranges of each offset; second, the length of subrange should be equal to each other to avoid biased estimation; finally, the overlapped subrange is not a good choice, since it results in biased estimation. Based on the above discussions, we choose the subranges with boundaries of 0.25 and -0.25 . Take δ_1 as an illustration, and the case for δ_2 follows similarly. The three cases are

$$\delta_1 \in \begin{cases} [-0.5, -0.25), & |Y_{L_1-0.25}| > |Y_{L_1}| \\ (0.25, 0.5], & |Y_{L_1+0.25}| > |Y_{L_1}|, \\ [-0.25, 0.25], & \text{otherwise.} \end{cases} \quad (43)$$

The reduced estimation range of δ_1 or δ_2 will help to reduce the MSE of $\hat{\theta}_1$ and $\hat{\theta}_2$. The details of the NIFM algorithm are shown in Tables 1 and 2.

TABLE 1. Estimation algorithm with θ_1 in three scenarios.

(I)	Obtain Y_k using N -DFT and find peak index L_1 ;
(II)	Choose the location of δ_1 using (??);
For $\delta_1 \in [-0.25, 0.25]$	
(III)	Obtain $\hat{\theta}_1$ using (??)–(??);
For $\delta_1 \in [-0.5, -0.25]$	
(III.1)	Update observations y_n using $y_n \exp\left(j\frac{\pi}{N}n\right)$;
(III.2)	Calculate new Y_{L_1} and $Y_{L_1\pm 1}$ using (??)–(??);
(III.3)	Obtain $\hat{\theta}_1$ using (??)–(??);
For $\delta_1 \in (0.25, 0.5]$	
(III.1)	Update observations y_n using $y_n \exp\left(-j\frac{\pi}{N}n\right)$;
(III.2)	Calculate new Y_{L_1} and $Y_{L_1\pm 1}$ using (??)–(??);
(III.3)	Obtain $\hat{\theta}_1$ using (??)–(??);

$$\begin{bmatrix} \frac{r_1}{D_3} + \frac{r_2}{D_2} - Br_0 & \frac{C_2 r_1}{D_3} + \frac{C_3 r_2}{D_2} - BC_4 r_0 & \frac{C_1 r_1}{D_3} - \frac{C_1 r_2}{D_2} \\ \frac{\ell_1}{D_2} + \frac{\ell_2}{D_3} - B\ell_0 & \frac{C_1 \ell_1}{D_2} - \frac{C_1 \ell_2}{D_3} & BC_4 \ell_0 - \frac{C_3 \ell_1}{D_2} - \frac{C_2 \ell_2}{D_3} \end{bmatrix} \cdot \begin{bmatrix} \mu_1 \mu_2 \\ \mu_1 \\ \mu_2 \end{bmatrix} = - \begin{bmatrix} \frac{C_1 C_2 r_1}{D_3} - \frac{C_1 C_3 r_2}{D_2} \\ \frac{D_3}{C_1 C_2 \ell_2} - \frac{D_2}{C_1 C_3 \ell_1} \\ \frac{D_3}{D_3} - \frac{D_2}{D_2} \end{bmatrix}. \quad (27)$$

$$\mathbf{x} = \begin{bmatrix} \text{Re}\{Y_{L_2}\} \\ \text{Re}\left\{\exp\left(j\frac{\pi}{N}\right)Y_{L_2-1}\right\} \\ \text{Re}\left\{\exp\left(-j\frac{\pi}{N}\right)Y_{L_2+1}\right\} \end{bmatrix}, \quad \mathbf{z} = \begin{bmatrix} \text{Re}\{Y_{L_1}\} \\ \text{Re}\left\{\exp\left(j\frac{\pi}{N}\right)Y_{L_1-1}\right\} \\ \text{Re}\left\{\exp\left(-j\frac{\pi}{N}\right)Y_{L_1+1}\right\} \end{bmatrix}, \quad (32)$$

$$\mathbf{A} = \begin{bmatrix} B^2 C_4 & \frac{B(C_1 + C_4)}{D_3} & \frac{B(C_1 - C_4)}{D_2} \\ -\frac{BC_3}{D_2} & \frac{D_3}{C_1 + C_3} & \frac{D_2}{C_3 - C_1} \\ -\frac{BC_2}{D_3} & \frac{D_2 D_3}{C_1 + C_2} & \frac{D_2^2}{C_2 - C_1} \end{bmatrix}, \quad (33)$$

$$\mathbf{B} = \begin{bmatrix} B^2 C_4^2 & -\frac{BC_2(C_1 + C_4)}{D_3} & \frac{BC_3(C_1 - C_4)}{D_2} \\ -\frac{BC_3(C_1 + C_4)}{D_2} & \frac{(C_1 + C_2)(C_1 + C_3)}{D_2 D_3} & \frac{C_3^2 - C_1^2}{D_2^2} \\ \frac{BC_2(C_1 - C_4)}{D_3} & \frac{C_2^2 - C_1^2}{D_3^2} & \frac{(C_1 - C_3)(C_1 - C_2)}{D_2 D_3} \end{bmatrix}, \quad (34)$$

$$\mathbf{C} = \begin{bmatrix} 0 & 0 & 0 \\ -\frac{BC_1 C_3 C_4}{D_2} & \frac{C_1 C_2 (C_1 + C_3)}{D_2 D_3} & \frac{C_1 C_3 (C_3 - C_1)}{D_2^2} \\ \frac{BC_1 C_2 C_4}{D_3} & -\frac{C_1 C_2 (C_1 + C_2)}{D_3^2} & \frac{C_1 C_3 (C_1 - C_2)}{D_2 D_3} \end{bmatrix}, \quad (35)$$

$$\mathbf{D} = \begin{bmatrix} B^2 C_4 & -\frac{BC_2}{D_3} & -\frac{BC_3}{C_3 - C_1} \\ \frac{B(C_1 - C_4)}{D_2} & \frac{D_3}{C_2 - C_1} & \frac{D_2}{C_3 - C_1} \\ -\frac{B(C_1 + C_4)}{D_3} & \frac{D_2 D_3}{C_1 + C_2} & \frac{D_2^2}{C_1 + C_3} \end{bmatrix}, \quad (36)$$

$$\mathbf{W} = \begin{bmatrix} -B^2 C_4^2 & \frac{BC_2(C_4 - C_1)}{D_3} & \frac{BC_3(C_4 + C_1)}{D_2} \\ \frac{BC_3(C_4 - C_1)}{D_2} & \frac{(C_2 - C_1)(C_1 - C_2)}{D_2 D_3} & \frac{C_1^2 - C_3^2}{D_2^2} \\ \frac{BC_2(C_1 + C_4)}{D_3} & \frac{C_1^2 - C_2^2}{D_3^2} & -\frac{(C_1 + C_3)(C_1 + C_2)}{D_2 D_3} \end{bmatrix}, \quad (37)$$

$$\mathbf{Q} = \begin{bmatrix} 0 & \frac{BC_1 C_2 C_4}{D_3} & -\frac{BC_1 C_3 C_4}{D_2} \\ 0 & \frac{C_1 C_3 (C_1 - C_2)}{D_2 D_3} & \frac{C_1 C_3 (C_3 - C_1)}{D_2^2} \\ 0 & -\frac{C_1 C_2 (C_1 + C_2)}{D_3^2} & \frac{C_1 C_2 (C_1 + C_3)}{D_2 D_3} \end{bmatrix}. \quad (38)$$

III. PERFORMANCE AND COMPUTATIONAL COMPLEXITY ANALYSIS

A. BIAS AND VARIANCE ANALYSIS

In this section, we analyze the bias and variance of $\hat{\theta}_1$ and $\hat{\theta}_2$. To simplify the problem, our discussion focuses on the range of $\delta_1, \delta_2 \in [-0.25, 0.25]$. For the other subranges such as $\delta_1, \delta_2 \in [-0.5, -0.25]$, according to the subrange criterion in Section 2, we introduce two new variables $\delta_1^{new} = \delta_1 + 0.5$ and $\delta_2^{new} = \delta_2 + 0.5$ ($\delta_1^{new}, \delta_2^{new} \in [0, 0.25]$). With the use of analysis in this section as well as δ_1^{new} and δ_2^{new} , the variances of $\hat{\theta}_1$ and $\hat{\theta}_2$, corresponding to the case of $\delta_1, \delta_2 \in [-0.5, -0.25]$, can be derived.

Since $\mu_1 = \tan\left(\frac{\pi\delta_1}{N}\right)$ and $\mu_2 = \tan\left(\frac{\pi\delta_2}{N}\right)$, the variances of $\hat{\delta}_1$ and $\hat{\delta}_2$ can be derived by those of $\hat{\mu}_1$ and $\hat{\mu}_2$. To analyze the performance of $\hat{\mu}_2$, we shall first note that $\hat{\mu}_2$ is actually obtained by solving

$$f(\hat{\mu}_2) = 0, \quad (44)$$

where $f(\hat{\mu}_2) = \mu_2^2 (\mathbf{x}^T \mathbf{A} \mathbf{z}) + \mu_2 (\mathbf{x}^T \mathbf{B} \mathbf{z}) + \mathbf{x}^T \mathbf{C} \mathbf{z}$. According to the definitions in (32)–(38), we have

$$\mathbf{B} = \mathbf{A} \mathbf{H} + \mathbf{F} \mathbf{A}, \quad \mathbf{C} = \mathbf{F} \mathbf{A} \mathbf{H}, \quad (45)$$

TABLE 2. Estimation algorithm with θ_2 in three scenarios.

(I)	Obtain Y_k using N -DFT and find peak index L_2 ;
(II)	Choose the location of δ_2 using (??);
For $\delta_2 \in [-0.25, 0.25]$	
(III)	Obtain $\hat{\theta}_2$ using (??)–(??);
For $\delta_2 \in [-0.5, -0.25]$	
(III.1)	Update observations y_n using $y_n \exp(j \frac{\pi}{N} n)$;
(III.2)	Calculate new Y_{L_2} and $Y_{L_2 \pm 1}$ using (??)–(??);
(III.3)	Obtain $\hat{\theta}_2$ using (??)–(??);
For $\delta_2 \in (0.25, 0.5]$	
(III.1)	Update observations y_n using $y_n \exp(-j \frac{\pi}{N} n)$;
(III.2)	Calculate new Y_{L_2} and $Y_{L_2 \pm 1}$ using (??)–(??);
(III.3)	Obtain $\hat{\theta}_2$ using (??)–(??);

where

$$\mathbf{F} = \begin{bmatrix} 0 & 0 & 0 \\ 0 & C_1 & 0 \\ 0 & 0 & -C_1 \end{bmatrix}, \quad \mathbf{H} = \begin{bmatrix} C_4 & 0 & 0 \\ 0 & C_2 & 0 \\ 0 & 0 & C_3 \end{bmatrix}. \quad (46)$$

Combining (45)–(46), $f(\hat{\mu}_2)$ is given by

$$f(\hat{\mu}_2) = \mathbf{x}^T \mathbf{K} \mathbf{z} \quad (47)$$

where $\mathbf{K} = (\mu_2 \mathbf{I}_3 + \mathbf{F}) \mathbf{A} (\mu_2 \mathbf{I}_3 + \mathbf{H})$ with \mathbf{I}_3 denoting the 3×3 identity matrix.

Utilizing [29], the bias and MSE of $\hat{\mu}_2$ can be calculated by TSE on $f(\hat{\mu}_2)$ [30]:

$$\text{Bias}(\hat{\mu}_2) = E\{\hat{\mu}_2\} - \mu_2 \approx -\frac{E\{f(\mu_2)\}}{E\{f'(\mu_2)\}}, \quad (48)$$

$$\text{MSE}(\hat{\mu}_2) = E\{(\hat{\mu}_2 - \mu_2)^2\} \approx \frac{E\{(f(\mu_2))^2\}}{(E\{f'(\mu_2)\})^2}, \quad (49)$$

where $f'(\mu_2)$ is the first-order derivative of $f(\mu_2)$ on μ_2 and $E\{\cdot\}$ denotes the expectation operator.

We rewrite \mathbf{x} and \mathbf{z} in (32) as $\mathbf{x} = \mathbf{x}_s + \mathbf{x}_q$ and $\mathbf{z} = \mathbf{z}_s + \mathbf{z}_q$, where \mathbf{x}_s and \mathbf{z}_s denote the signal parts, while \mathbf{x}_q and \mathbf{z}_q are the noise parts. It is also worth pointing out that \mathbf{x}_q and \mathbf{z}_q are IID noise terms with variance σ^2 . Then $f(\mu_2)$ in (47) can be expressed as

$$f(\mu_2) = \mathbf{x}_s^T \mathbf{K} \mathbf{z}_s + \mathbf{x}_q^T \mathbf{K} \mathbf{z}_q + \mathbf{x}_s^T \mathbf{K} \mathbf{z}_q + \mathbf{x}_q^T \mathbf{K} \mathbf{z}_s, \quad (50)$$

According to the Appendix, we have

$$\mathbf{x}_s^T \mathbf{K} \mathbf{z}_s = 0. \quad (51)$$

Utilizing (25)–(26) and the definition of $f(\mu_2)$, we obtain

$$E\{f(\mu_2)\} = \mathbf{x}_s^T \mathbf{K} \mathbf{z}_s = 0, \quad (52)$$

$$E\{f'(\mu_2)\} = \mathbf{x}_s^T \mathbf{L} \mathbf{z}_s, \quad (53)$$

$$E\{(f(\mu_2))^2\} = \sigma^2(N\sigma^2 \text{tr}(\mathbf{K}^T \mathbf{K}) + \mathbf{x}_s^T \mathbf{K} \mathbf{K}^T \mathbf{x}_s + N \mathbf{z}_s^T \mathbf{K}^T \mathbf{K} \mathbf{z}_s), \quad (54)$$

where $\text{tr}\{\cdot\}$ denotes the matrix trace and

$$\mathbf{L} = \mathbf{A} (\mu_2 \mathbf{I}_3 + \mathbf{H}) + (\mu_2 \mathbf{I}_3 + \mathbf{F}) \mathbf{A}. \quad (55)$$

According to (52) and (54), (48) is calculated as

$$\text{Bias}(\hat{\mu}_2) \approx 0. \quad (56)$$

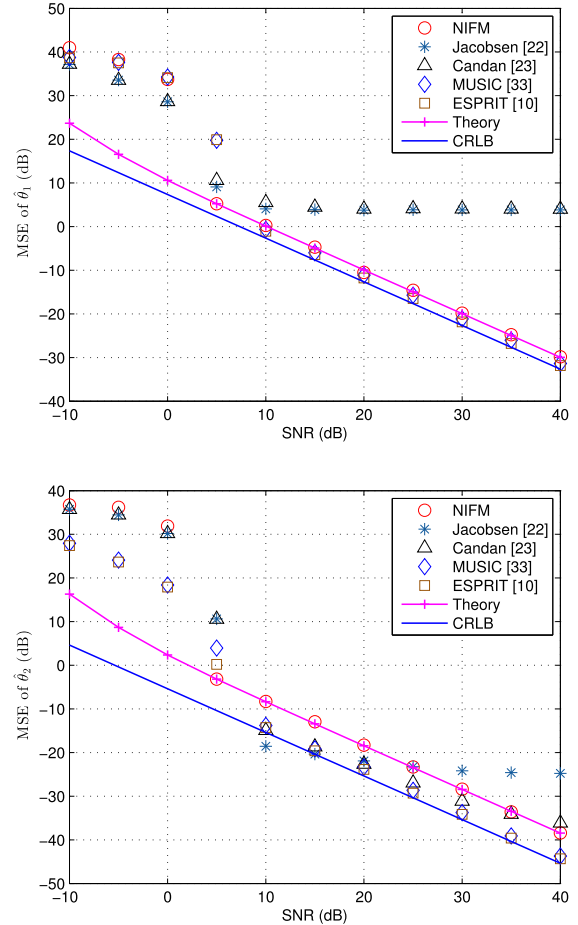


FIGURE 2. Mean squares error versus SNR.

With the use of (49) and (53)–(54), $\text{MSE}(\hat{\mu}_2)$ is expressed as

$$\text{MSE}(\hat{\mu}_2) \approx \sigma^2 \frac{N\sigma^2 \text{tr}(\mathbf{K}^T \mathbf{K}) + \mathbf{x}_s^T \mathbf{K} \mathbf{K}^T \mathbf{x}_s + N \mathbf{z}_s^T \mathbf{K}^T \mathbf{K} \mathbf{z}_s}{(\mathbf{x}_s^T \mathbf{L} \mathbf{z}_s)^2}, \quad (57)$$

Similarly, the bias and MSE of $\hat{\mu}_1$, are

$$\text{Bias}(\hat{\mu}_1) \approx 0, \quad (58)$$

$$\text{MSE}(\hat{\mu}_1) \approx \sigma^2 \frac{N\sigma^2 \text{tr}(\mathbf{M}^T \mathbf{M}) + \mathbf{x}_s^T \mathbf{M} \mathbf{M}^T \mathbf{x}_s + N \mathbf{z}_s^T \mathbf{M}^T \mathbf{M} \mathbf{z}_s}{(\mathbf{x}_s^T \mathbf{T} \mathbf{z}_s)^2}, \quad (59)$$

where

$$\mathbf{M} = \mathbf{G}_1 \times \mathbf{D} \times \mathbf{G}_2, \quad (60)$$

$$\mathbf{T} = \mathbf{D} \times \mathbf{G}_2 + \mathbf{G}_1 \times \mathbf{D}. \quad (61)$$

where

$$\mathbf{G}_1 = \begin{bmatrix} \mu_1 - C_4 & 0 & 0 \\ 0 & \mu_1 - C_3 & 0 \\ 0 & 0 & \mu_1 - C_2 \end{bmatrix}, \quad (62)$$

$$\mathbf{G}_2 = \begin{bmatrix} \mu_1 & 0 & 0 \\ 0 & \mu_1 + C_1 & 0 \\ 0 & 0 & \mu_1 - C_1 \end{bmatrix}. \quad (63)$$

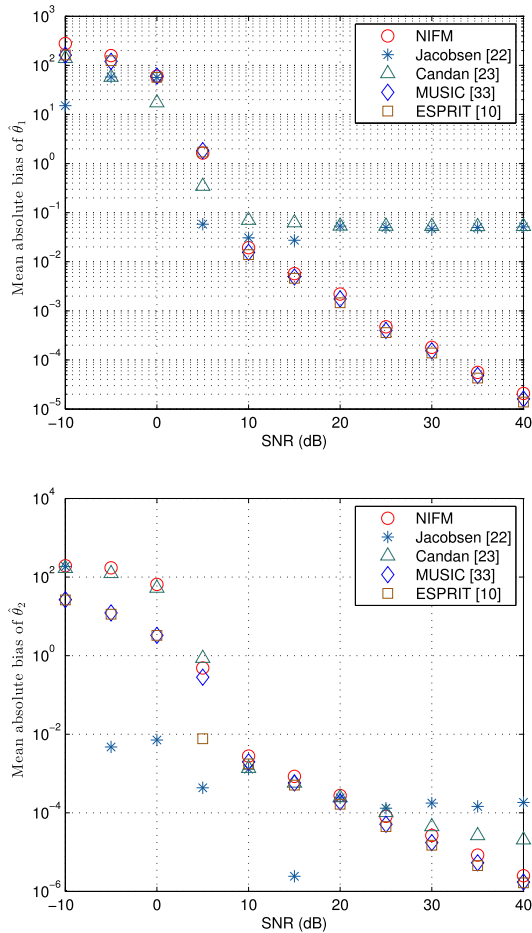


FIGURE 3. Absolute biases versus SNR.

Employing the definition in (41)–(42) and according to [31], the MSEs of $\hat{\theta}_1$ and $\hat{\theta}_2$, referred to as $MSE(\hat{\theta}_1)$ and $MSE(\hat{\theta}_2)$, have the forms of

$$MSE(\hat{\theta}_1) = \left(\frac{4}{(1 + \mu_1^2)^2 (\pi^2 - (\pi\theta_1)^2)} \right) MSE(\hat{\mu}_1), \quad (64)$$

$$MSE(\hat{\theta}_2) = \left(\frac{4}{(1 + \mu_2^2)^2 (\pi^2 - (\pi\theta_2)^2)} \right) MSE(\hat{\mu}_2). \quad (65)$$

B. COMPUTATIONAL COMPLEXITY ANALYSIS

The estimation steps of NIFM are summarized as follows:
 (1) Calculate the spectrum of observations using fast Fourier transform (FFT) with $\mathcal{O}(N \log_2(N))$ flops and search for the two magnitude peaks with $\mathcal{O}(N)$;
 (2) Estimate μ_1 and μ_2 using (39) and (40) twice;
 (3) Estimate the two DOA values $\hat{\theta}_1$ and $\hat{\theta}_2$ using Tables 1 and 2.

It is vivid that the dominant computational complexity is the FFT, and the peak search, which makes the algorithm complexity to be proportional to $\mathcal{O}(N(1 + \log_2(N)))$.

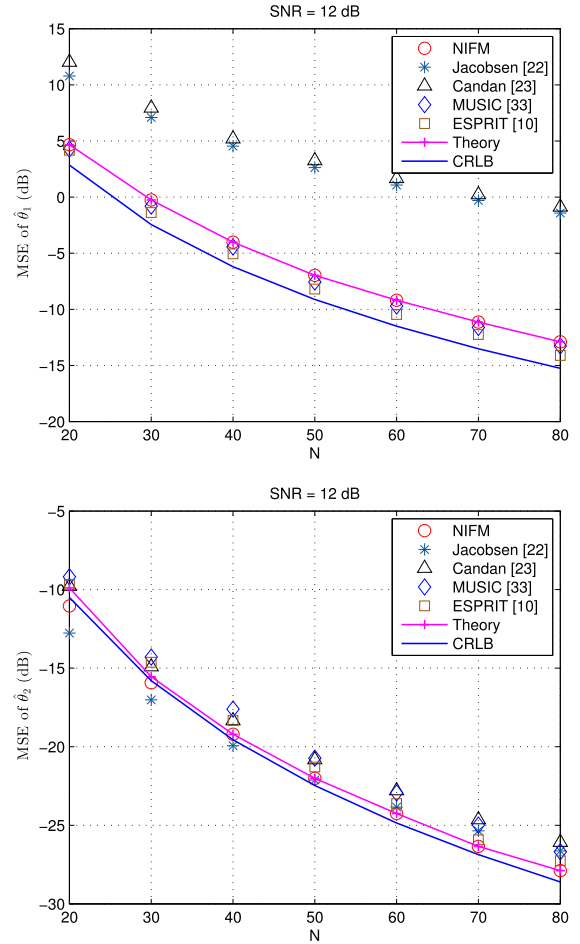


FIGURE 4. Mean squares error versus sensor number N .

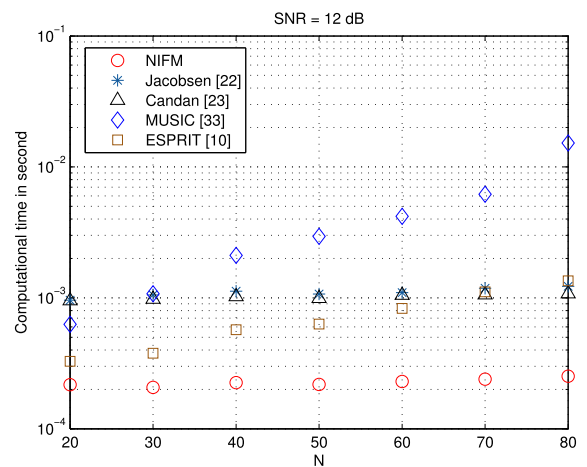


FIGURE 5. Computational times for different N .

IV. SIMULATIONS

To verify the performance of the interpolation formulas, computer simulations have been conducted. We employ the empirical MSEs and absolute biases of $\hat{\theta}_1$ and $\hat{\theta}_2$ as the performance metrics, which are defined as $E\{(\theta_p - \hat{\theta}_p)^2}$ and $|\hat{\theta}_p - E\{\hat{\theta}_p\}|$ with $p = 1, 2$, respectively. Two sources locating

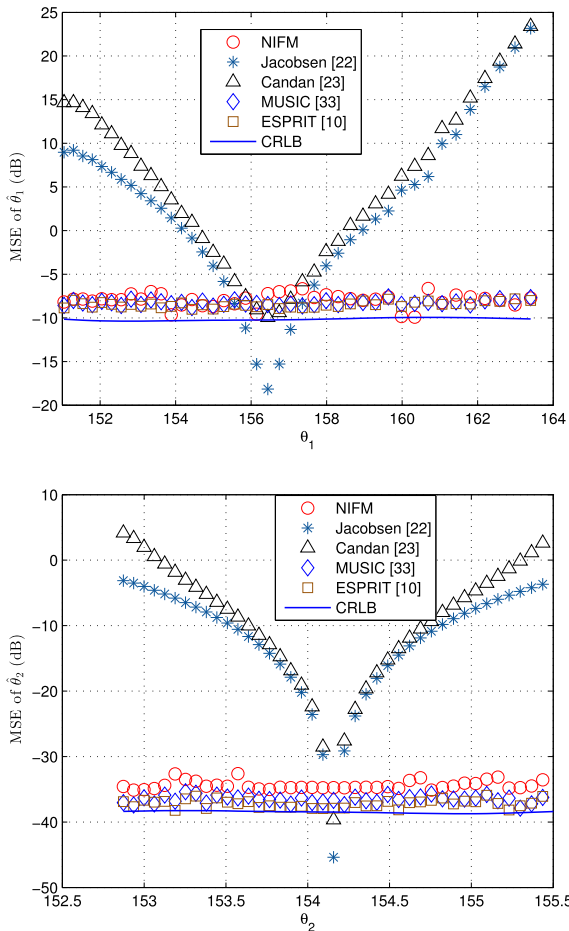


FIGURE 6. Mean squares error versus θ_1 or θ_2 .

at $\theta_1 = 158^\circ$ and $\theta_2 = 126^\circ$ are considered, whose powers are 1 and 4, respectively. And hence, the corresponding peak indices in model (2) are $L_1 = 2$ and $L_2 = 6$, while the offsets are $\delta_1 = -0.12$ and $\delta_2 = 0.018$. The Cramér-Rao lower bound (CRLB) [32] is included as the benchmark while comparisons with Jacobsen [22], Candan [23], MUSIC [33] and ESPRIT [10] methods are also provided. For Jacobsen algorithm, Hanning window is utilized with scaling parameter 0.55. All results are simulated using Matlab running on Intel(R) Core(TM) i7-4790 CPU@3.60GHz and Windows 7 for 1000 Monte Carlo trials with $N = 24$ sensors.

First of all, we investigate the performance of the proposed method in different noise conditions. The MSEs and absolute biases of $\hat{\theta}_1$ and $\hat{\theta}_2$ versus SNR are plotted in Figures 2 and 3. It can be observed in Figure 2 that although the proposed method is suboptimal, it can approach CRLB faster than other optimal estimators in the case of low SNR. Figure 3 also verifies this finding since our approach can provide stable estimates when $\text{SNR} > 5$ dB, but those of the other methods are only reliable for $\text{SNR} > 10$ dB. It is noted that Jacobsen and Candan algorithms are biased in estimating θ_1 and θ_2 , since they are devised with the assumption of single-target model.

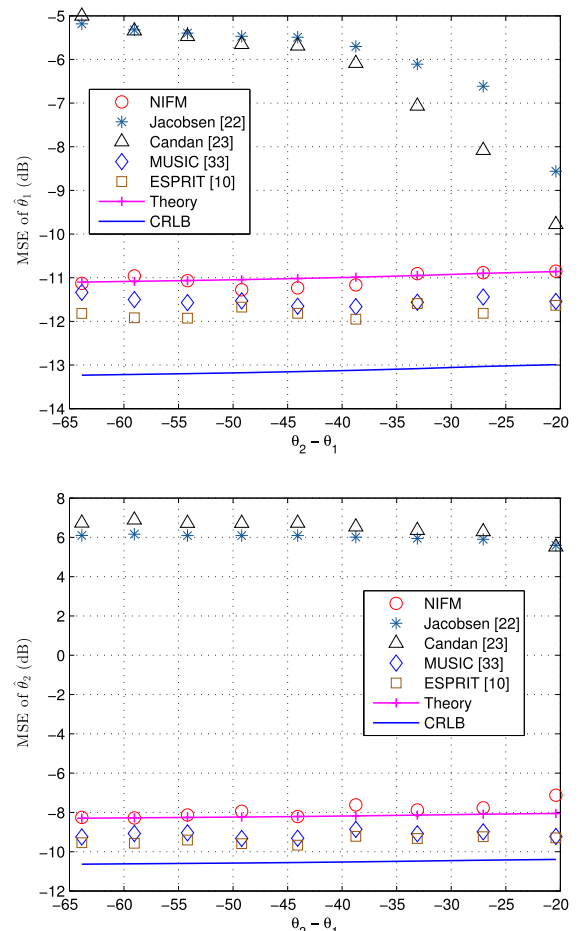


FIGURE 7. Mean squares error versus L .

Second, the MSEs and the computational cost versus sensor number N are plotted in Figures 4 and 5 for the cases of $\text{SNR} = 12$ dB with $N \in [20, 80]$. Here the parameters L_1, L_2, δ_1 and δ_2 are same with the previous experiment. Here, the DOAs are $\theta_1 \in [156^\circ, 168^\circ]$ and $\theta_2 \in [120^\circ, 151^\circ]$. The stopwatch timer is utilized to measure the run times of all methods. It is indicated that in the case of nearly optimal estimation performance, the complexity of the proposed method is significantly lower than the MUSIC and ESPRIT. While the performance of NIFM is more accurate than the Jacobsen and Candan schemes with approximately the same computational cost. Moreover, as the number of sensors increases, the computational complexity of NIFM almost does not change while other methods grow linearly in high rate.

Third, the estimation performance for different θ_1 and θ_2 is examined with $L_1 = 2, L_2 = 6$ and the SNR is 12 dB. For different θ_1 in $[151^\circ, 163^\circ]$, θ_2 is fixed to 126° , while in the case of different θ_2 in $[152^\circ, 156^\circ]$, $\theta_1 = 168^\circ$. It is shown in Figure 6 that the MSEs of all methods approach CRLB in all values of θ_1 and θ_2 , except the Jacobsen and Candan algorithms. With the use of the criterion in Table 1, the gap between the proposed method and CRLB is less than 3.5 dB in Figure 6, and does not change much as θ_1 and θ_2 change.

$$\begin{bmatrix} \frac{g_1}{D_3} + \frac{g_2}{D_2} - Bg_0 & \frac{C_2 g_1}{D_3} + \frac{C_3 g_2}{D_2} - BC_4 g_0 \\ \frac{h_1}{D_2} + \frac{h_2}{D_3} - Bh_0 & \frac{C_1 h_1}{D_2} - \frac{C_1 h_2}{D_3} \\ BC_4 h_0 - \frac{C_3 h_1}{D_2} - \frac{C_2 h_2}{D_3} & \frac{C_1 g_1}{D_3} - \frac{C_1 g_2}{D_2} \end{bmatrix} \cdot \begin{bmatrix} \mu_1 \mu_2 \\ \mu_1 \\ \mu_2 \end{bmatrix} = - \begin{bmatrix} \frac{C_1 C_2 r_1}{D_3} - \frac{C_1 C_3 r_2}{D_2} \\ \frac{D_3}{C_1 C_2 \ell_2} - \frac{D_2}{C_1 C_3 \ell_1} \end{bmatrix}, \quad (74)$$

Finally, the estimation performance in the case of different DOAs is studied. We vary θ_2 from 95° to 139° , when θ_1 is fixed to 158° . Figure 7 shows that in the scenario of closely-spaced peaks, our method can also perform well, indicating the stability of the proposed method. It is worth pointing out that in the case of increasing θ_2 , the MSEs of the Jacobsen and Candan algorithms become larger. This is because these two methods assume that the signal model is single-target and ignore the influence in dual-target scenario.

In summary, in the scenarios of different SNR, N , θ_1 and θ_2 , the proposed method is nearly optimal, and it has the lowest computational complexity with unbiased estimation performance.

V. CONCLUSION

In this paper, a fast and simple DOA estimator, referred to as NIFM, using the magnitudes of DFT are developed, which has lower computational complexity than that of existing methods. Theoretical analysis is investigated to show the near optimality of the proposed algorithm. Computer simulations show that the performance of the proposed algorithm is similar to that of Jacobsen, Candan, MUSIC and ESPRIT, while it can achieve much lower computational complexity. In particular, the computational complexity of NIFM is not sensitive to data set size increment, when compared to the other algorithms discussed in this paper. It is worth pointing that although our work focuses on the two-target DOA estimation in single-snapshot, it can be also extended to the scenario of multiple targets, even with multiple snapshots.

APPENDIX

Utilizing (32), \mathbf{x}_s and \mathbf{z}_s are

$$\mathbf{x}_s = \begin{bmatrix} Re \{S_{L_2}\} \\ Re \left\{ \exp \left(j \frac{\pi}{N} \right) S_{L_2-1} \right\} \\ Re \left\{ \exp \left(-j \frac{\pi}{N} \right) S_{L_2+1} \right\} \end{bmatrix} \quad (66)$$

$$\mathbf{z}_s = \begin{bmatrix} Re \{S_{L_1}\} \\ Re \left\{ \exp \left(j \frac{\pi}{N} \right) S_{L_1-1} \right\} \\ Re \left\{ \exp \left(-j \frac{\pi}{N} \right) S_{L_1+1} \right\} \end{bmatrix} \quad (67)$$

where S_l has the form of

$$S_{L_1} = \frac{\gamma_1}{\sin \left(\frac{\pi \delta_1}{N} \right)} + \frac{\gamma_2}{\sin \left(\frac{\pi(L+\delta_2)}{N} \right)},$$

$$S_{L_1-1} = \exp \left(-\frac{j\pi}{N} \right) \left(\frac{\gamma_1}{\sin \left(\frac{\pi(\delta_1+1)}{N} \right)} + \frac{\gamma_2}{\sin \left(\frac{\pi(L+\delta_2+1)}{N} \right)} \right),$$

$$S_{L_1+1} = \exp \left(\frac{j\pi}{N} \right) \left(\frac{\gamma_1}{\sin \left(\frac{\pi(\delta_1-1)}{N} \right)} + \frac{\gamma_2}{\sin \left(\frac{\pi(L+\delta_2-1)}{N} \right)} \right), \quad (68)$$

$$S_{L_2} = \frac{\alpha_1}{\sin \left(\frac{\pi(-L+\delta_1)}{N} \right)} + \frac{\alpha_2}{\sin \left(\frac{\pi \delta_2}{N} \right)},$$

$$S_{L_2-1} = \exp \left(-\frac{j\pi}{N} \right) \left(\frac{\alpha_1}{\sin \left(\frac{\pi(-L+\delta_1+1)}{N} \right)} + \frac{\alpha_2}{\sin \left(\frac{\pi(\delta_2+1)}{N} \right)} \right),$$

$$S_{L_2+1} = \exp \left(\frac{j\pi}{N} \right) \left(\frac{\alpha_1}{\sin \left(\frac{\pi(-L+\delta_1-1)}{N} \right)} + \frac{\alpha_2}{\sin \left(\frac{\pi(\delta_2-1)}{N} \right)} \right). \quad (69)$$

with

$$\alpha_1 = A_1 \exp \left(j\pi \frac{L}{N} \right) \exp \left(j\pi \delta_1 \frac{N-1}{N} \right) \sin(\pi \delta_1), \quad (70)$$

$$\alpha_2 = A_2 \exp \left(j\pi \delta_2 \frac{N-1}{N} \right) \sin(\pi \delta_2). \quad (71)$$

Equations (68)-(69) satisfy

$$\begin{aligned} & \sin \left(\frac{\pi(\delta_1+1)}{N} \right) \sin \left(\frac{\pi(L+\delta_2+1)}{N} \right) \exp \left(\frac{j\pi}{N} \right) S_{L_1-1} \\ & + \sin \left(\frac{\pi(\delta_1-1)}{N} \right) \sin \left(\frac{\pi(L+\delta_2-1)}{N} \right) \exp \left(-\frac{j\pi}{N} \right) S_{L_1+1} \\ & = 2 \cos \left(\frac{\pi}{N} \right) \sin \left(\frac{\pi \delta_1}{N} \right) \sin \left(\frac{\pi(L+\delta_2)}{N} \right) S_{L_1}, \end{aligned} \quad (72)$$

$$\begin{aligned} & \sin \left(\frac{\pi(\delta_1+1-L)}{N} \right) \sin \left(\frac{\pi(\delta_2+1)}{N} \right) \exp \left(\frac{j\pi}{N} \right) S_{L_2-1} \\ & + \sin \left(\frac{\pi(\delta_1-1-L)}{N} \right) \sin \left(\frac{\pi(\delta_2-1)}{N} \right) \exp \left(-\frac{j\pi}{N} \right) S_{L_2+1} \\ & = 2 \cos \left(\frac{\pi}{N} \right) \sin \left(\frac{\pi(\delta_1-L)}{N} \right) \sin \left(\frac{\pi \delta_2}{N} \right) S_{L_2}. \end{aligned} \quad (73)$$

Employing the definitions of μ_1 and μ_2 as well as (28)–(29) and (72)–(73), we have (74), shown at the top of this page, where

$$\begin{aligned} g_0 &= Re \{S_{L_1}\}, \quad h_0 = Re \{S_{L_2}\} \\ g_1 &= Re \left\{ \exp \left(j \frac{\pi}{N} \right) S_{L_1-1} \right\}, \\ g_2 &= Re \left\{ \exp \left(-j \frac{\pi}{N} \right) S_{L_1+1} \right\}, \\ h_1 &= Re \left\{ \exp \left(j \frac{\pi}{N} \right) S_{L_2-1} \right\}, \\ h_2 &= Re \left\{ \exp \left(-j \frac{\pi}{N} \right) S_{L_2+1} \right\}. \end{aligned} \quad (74)$$

To remove the term $\mu_1\mu_2$, with the use of (66)-(67), (74) can be rewritten as

$$\mu_2^2 (\mathbf{x}_s^T \mathbf{A} \mathbf{z}_s) + \mu_2 (\mathbf{x}_s^T \mathbf{B} \mathbf{z}_s) + \mathbf{x}_s^T \mathbf{C} \mathbf{z}_s = 0, \quad (75)$$

Since $\mathbf{x}_s \mathbf{K} \mathbf{z}_s = \mu_2^2 (\mathbf{x}^T \mathbf{A} \mathbf{z}) + \mu_2 (\mathbf{x}^T \mathbf{B} \mathbf{z}) + \mathbf{x}^T \mathbf{C} \mathbf{z}$, we have

$$\mathbf{x}_s^T \mathbf{K} \mathbf{z}_s = 0. \quad (76)$$

REFERENCES

- [1] S. D. Blunt, K. J. Smith, and K. Gerlach, "Doppler-compensated adaptive pulse compression," in *Proc. IEEE Conf. Radar*, Verona, NY, USA, Apr. 2006, pp. 114–119.
- [2] J. C. Preisig, "Performance analysis of adaptive equalization for coherent acoustic communications in the time-varying ocean environment," *J. Acoust. Soc. Amer.*, vol. 118, no. 1, pp. 263–278, Jul. 2005.
- [3] H. Wang, L. Wan, M. Dong, K. Ota, and X. Wang, "Assistant vehicle localization based on three collaborative base stations via SBL-based robust DOA estimation," *IEEE Internet Things J.*, to be published. doi: 10.1109/JIOT.2019.2905788.
- [4] Z. Zheng, W.-Q. Wang, Y. Kong, and Y. D. Zhang, "MISC array: A new sparse array design achieving increased degrees of freedom and reduced mutual coupling effect," *IEEE Trans. Signal Process.*, vol. 67, no. 7, pp. 1728–1741, Apr. 2019.
- [5] X. Wang, L. Wang, X. Li, and G. Bi, "Nuclear norm minimization framework for DOA estimation in MIMO radar," *Signal Process.*, vol. 135, pp. 147–152, Jun. 2017.
- [6] P. S. Naidu, *Sensor Array Signal Processing*. Boca Raton, FL, USA: CRC Press, 2000.
- [7] X. Wang, M. Huang, C. Shen, and D. Meng, "Robust vehicle localization exploiting two based stations cooperation: A MIMO radar perspective," *IEEE Access*, vol. 6, pp. 48747–48755, 2018.
- [8] C. Qian, Y. Shi, L. Huang, and H. C. So, "Robust harmonic retrieval via block successive upper-bound minimization," *IEEE Trans. Signal Process.*, vol. 66, no. 23, pp. 6310–6324, Oct. 2018.
- [9] S. M. Kay, *Fundamentals of Statistical Signal Processing: Estimation Theory*. Englewood Cliffs, NJ, USA: Prentice-Hall, 1993.
- [10] P. Stoica and R. Moses, *Spectral Analysis of Signals*. Upper Saddle River, NJ, USA: Prentice-Hall, 2005.
- [11] J. Capon, "High resolution frequency-wavenumber spectrum analysis," *Proc. IEEE*, vol. 57, no. 8, pp. 1408–1418, Aug. 1969.
- [12] P. Handel, P. Stoica, and T. Soderstrom, "Capon method for doa estimation: Accuracy and robustness aspects," in *Proc. IEEE Winter Workshop Nonlinear Digit. Signal Process.*, Tampere, Finland, Jan. 1993, pp. 1–3.
- [13] P. Stoica, P. Händel, and T. Söderström, "Study of Capon method for array signal processing," *Circuits, Syst. Signal Process.*, vol. 14, no. 6, pp. 749–770, Nov. 1995.
- [14] P. Stoica and A. Nehorai, "MUSIC, maximum likelihood, and Cramer-Rao bound," *IEEE Trans. Acoust., Speech, Signal Process.*, vol. 38, no. 5, pp. 720–741, May 1989.
- [15] R. O. Schmidt, "Multiple emitter location and signal parameter estimation," *IEEE Trans. Antennas Propag.*, vol. AP-34, no. 3, pp. 276–280, Mar. 1986.
- [16] R. Roy, A. Paulraj, and T. Kailath, "ESPRIT—A subspace rotation approach to estimation of parameters of cisoids in noise," *IEEE Trans. Acoust., Speech, Signal Process.*, vol. ASSP-34, no. 5, pp. 1340–1342, Oct. 1986.
- [17] J. Li and P. Stoica, "An adaptive filtering approach to spectral estimation and SAR imaging," *IEEE Trans. Signal Process.*, vol. 44, no. 6, pp. 1469–1484, Jun. 1996.
- [18] D. J. Russell and R. D. Palmer, "Application of APES to adaptive arrays on the CDMA reverse channel," *IEEE Trans. Veh. Technol.*, vol. 53, no. 1, pp. 3–17, Jan. 2004.
- [19] B. G. Quinn, "Estimation of frequency, amplitude, and phase from the DFT of a time series," *IEEE Trans. Signal Process.*, vol. 45, no. 3, pp. 814–817, Mar. 1997.
- [20] S. Provencher, "Estimation of complex single-tone parameters in the DFT domain," *IEEE Trans. Signal Process.*, vol. 58, no. 7, pp. 3879–3883, Jul. 2010.
- [21] C. Candan, "Fine resolution frequency estimation from three DFT samples: Case of windowed data," *Signal Process.*, vol. 114, pp. 245–250, Sep. 2015.
- [22] E. Jacobsen and P. Kootsookos, "Fast, accurate frequency estimators," *IEEE Signal Process. Mag.*, vol. 24, no. 3, pp. 123–125, May 2007.
- [23] C. Candan, "Analysis and further improvement of fine resolution frequency estimation method from three DFT samples," *IEEE Signal Process. Lett.*, vol. 20, no. 9, pp. 913–916, Sep. 2013.
- [24] U. Orguner and C. Candan, "A fine-resolution frequency estimator using an arbitrary number of DFT coefficients," *Signal Process.*, vol. 105, no. 10, pp. 17–21, Dec. 2014.
- [25] A. Karbasi and A. Sugiyama, "A new DOA estimation method using a circular microphone array," in *Proc. 15th Eur. Signal Process. Conf.*, Poznan, Poland, Sep. 2007, pp. 778–782.
- [26] K. W. Chan and H. C. So, "An exact analysis of Pisarenko's single-tone frequency estimation algorithm," *Signal Process.*, vol. 83, no. 3, pp. 685–690, Mar. 2003.
- [27] H. L. Van Trees, *Optimum Array Processing: Part IV of Detection, Estimation, and Modulation Theory*. New York, NY, USA: Wiley, 2002.
- [28] A. Uncini, *Fundamentals of Adaptive Signal Processing*. New York, NY, USA: Springer, 2015.
- [29] V. H. MacDonald and P. M. Schultheiss, "Optimum passive bearing estimation in a spatially incoherent noise environment," *J. Acoust. Soc. Amer.*, vol. 46, no. 1A, pp. 37–43, 1969.
- [30] H. C. So, Y. T. Chan, K. C. Ho, and Y. Chen, "Simple formulae for bias and mean square error computation," *IEEE Signal Process. Mag.*, vol. 30, no. 4, pp. 162–165, Jul. 2013.
- [31] A. Papoulis and S. U. Pillai, *Probability, Random Variables and Stochastic Processes*. New York, NY, USA: McGraw-Hill, 1991.
- [32] A. Nehorai and E. Paldi, "Acoustic vector-sensor array processing," *IEEE Trans. Signal Process.*, vol. 42, no. 9, pp. 2481–2491, Sep. 1994.
- [33] L. Huang, Y. Wu, H. C. So, Y. Zhang, and L. Huang, "Multidimensional sinusoidal frequency estimation using subspace and projection separation approaches," *IEEE Trans. Signal Process.*, vol. 60, no. 10, pp. 5536–5543, Oct. 2012.



processing, frequency estimation, machine learning, and their applications.



ANNIE HIN CHEUNG KO is currently a Senior Lecturer with the School of Professional Education and Executive Development, The Hong Kong Polytechnic University. She has been elected as a Fellow of the World Business Institute, Australia, since 2014. She was a recipient of the CPCE Dean's Award for Outstanding Teaching Performance (2013–2014).



WING SHAN TAM (SM'16) was born in Hong Kong. She received the Ph.D. degree in electronic engineering from the City University of Hong Kong. She has been working in different telecommunication and semiconductor companies, since 2004, and is currently the Engineering Manager of the Canaan Semiconductor Limited, where she works on both advance CMOS sensor design, and high power MOSFET and IGBT processes development. She has participated in professional services actively, in which she has been a Researcher in different universities, since 2007. She has been the invited speaker for different talks and seminars in numerous international conferences. She is also the author of two textbooks published by the Wiley-IEEE. Her research interests include multimedia signal processing and mixed-signal integrated circuit design for data conversion and power-management, and fabrication process and new device structure development. She has been serving as a Guest Editor in multiple international journals, since 2014. She is the founding Editor of the journal *Solid State Electronics Letters*, since 2017.



CHI-WAH KOK (SM'99) was born in Hong Kong. He received the Ph.D. degree from the University of Wisconsin–Madison. Since 1992, he has been working with various semiconductor companies, research institutions, and universities, which include AT&T Labs Research, Holmdel, USA; the SONY U.S. Research Labs; Stanford University; The Hong Kong University of Science and Technology; The Hong Kong Polytechnic University; City University of Hong Kong, and Lattice Semiconductor.

He was the MPEG (MPEG4) and JPEG (JPEG 2000) Standards Committee Member. He also is the author of three books by Prentice Hall and Wiley-IEEE, and has written numerous papers on digital signal processing, multimedia signal processing, and CMOS circuits, devices, fabrication process, and reliability. He is the founding Editor-in-Chief of the journal *Solid State Electronics Letters*, since 2017.



HING CHEUNG SO (S'90–M'95–SM'07–F'15) was born in Hong Kong. He received the B.Eng. degree from the City University of Hong Kong and the Ph.D. degree from The Chinese University of Hong Kong, both in electronic engineering, in 1990 and 1995, respectively.

From 1990 to 1991, he was an Electronic Engineer with the Research and Development Division, Everex Systems Engineering Ltd., Hong Kong. He was a Postdoctoral Fellow with The Chinese University of Hong Kong (1995–1996). From 1996 to 1999, he was a Research Assistant Professor with the Department of Electronic Engineering, City University of Hong Kong, where he is currently a Professor. His research interests include detection and estimation, fast and adaptive algorithms, multidimensional harmonic retrieval, robust signal processing, source localization, and sparse approximation. In addition, he was an elected member in Signal Processing Theory and Methods Technical Committee (2011–2016) of the IEEE Signal Processing Society, where he was the Chair in the awards subcommittee (2015–2016). He has been on the editorial boards of the *IEEE Signal Processing Magazine* (2014–2017), the IEEE TRANSACTIONS ON SIGNAL PROCESSING (2010–2014), the *Signal Processing*, since 2010, and the *Digital Signal Processing*, since 2011. He was also the Lead Guest Editor of the IEEE JOURNAL OF SELECTED TOPICS IN SIGNAL PROCESSING, the special issue on Advances in Time/Frequency Modulated Array Signal Processing, in 2017.

• • •